Dynamics of disk-like particles in turbulent vertical channel flow

Wenjun Yuan [a, b], Helge I. Andersson[b], Lihao Zhao [b, c] *, Niranjan Reddy Challabotla [b], Jianqiang Deng [a]

a. *Department of Process Equipment and Control Engineering, Xi'an Jiaotong University, Xi'an 710049, China*

b. *Department of Energy and Process Engineering, Norwegian University of Science and Technology, Trondheim 7491, Norway*

c. *Department of Engineering Mechanics, Tsinghua University, Beijing 10084, China*

* Corresponding author.
  E-mail addresses: zhaolihao@tsinghua.edu.cn

Abstract: The dynamical behavior of inertial disk-like particles in turbulent vertical channel flow is investigated by an Eulerian-Lagrangian point-particle approach. Gravity effects on distribution, translation, rotation and orientation statistics of non-spherical particles modeled as oblate spheroids have been studied both in an upward and a downward flow and compared with results obtained in the absence of gravity. Altogether 12 different particle classes have been studied, with inertia and shape parameterized by means of Stokes number St and aspect ratio $\lambda \leq 1$. The St =5 disk-like particles distribute more evenly across the channel in upward than in downward flow. The gravity effect on the particle concentration diminishes with large inertia and the spheroid shape has only a modest influence. Although the gravity significantly affects the streamwise and wall-normal mean slip velocities with increasing inertia, the particle shape rarely has any impact on the translational motion, except for the mean wall-normal velocity. The fluctuations of the velocity of disk-like particles are mainly ascribed to inertia, whereas the gravity and shape only have marginal effects. The presence of gravity is moreover found to have a negligible effect on the particles' orientation and rotation, in spite of the striking effect of λ on the orientation and rotation seen in the near-wall region. The tendency of the disks to align their symmetry axis orthogonal to the fluid vorticity in the channel center is stronger for particles with modest inertia. In the near-wall region, however, oblate spheroids preferentially align with the fluid vorticity for St $\gg$1. The observed behavior is believed to be caused by the influence of the gravity force on the turbophoresis; i.e. that inertial particles move towards low-turbulence regions.

Keywords: Disk-like particles; Turbulent flow; Gravity; Direct Numerical Simulation; Lagrangian point-particle approach

1.   Introduction

Turbulent suspension flows with solid particles exist widely in industrial and natural processes, such as fluidization reacting in chemical plants (Loranger et al., 2009), soot emission in a combustor (Levin et al., 2016), sand storms in the atmosphere (Akhlaq et al., 2012), and pollutant dispersion in the environment (Tominaga and Stathopoulos, 2013). There are a large number of studies focusing on spherical particles in wall-bounded turbulent flows through numerical solutions (Marchioli and Soldati, 2002; Arcen et al., 2006; Mortensen et al., 2007; Marchioli et al., 2008; Eaton, 2009; Kuerten, 2016). However, particle shapes in realistic applications are usually not confined to spheres. Non-spherical particles suspended in fluid turbulence have received less attention compared to spherical particles.

Beyond the complexity of multiphase flows with spherical particles and of turbulence (Balachandar and Eaton, 2010; Voth and Soldati, 2017), forces and torques that depend on particle orientation should be considered for non-spherical particle suspensions. According to the original mathematical analysis by Jeffery (1922) and the following contributions (Brenner, 1964; Harper and Chang, 1968; Gallily and Cohen, 1979), the hydrodynamic drag force and torque for an arbitrary ellipsoidal particle suspended in a creeping shear flow are mathematically tractable. This provides a reliable method to perform numerical investigations on sub-Kolmogorov inertial ellipsoids in turbulent flows (Andersson and Soldati, 2013; Voth and Soldati, 2017). In general, most of the existing papers concerning non-spherical particles have considered regular axisymmetric shapes, i.e. either prolate (fiber-like) or oblate (disk-like) spheroids, with a single aspect ratio defined as the ratio between the length of the symmetry axis and the two equal axes. Nonetheless, the majority of these studies have been devoted to fiber-like particles due to their relevance in paper making (Lundell et al., 2011), biomass combustion (Ma et al., 2007) and polymer processing (Han, 2012). The disk-like particles occur as cells in blood vessels (Kleinstreuer and Feng, 2013), ice crystals in clouds (Siewert et al., 2014) and phytoplankton in the ocean (Guasto et al., 2012), and have been little investigated.

Among the previous work for fiber-like particles, Zhang et al. (2001) were the first to investigate the transport and deposition of inertial prolate spheroids in turbulent channel flow using direct numerical simulations (DNSs), and pointed out that the coherent vortical structure plays an important role on the distribution of ellipsoids. Subsequently, Mortensen et al. (2008b, a) and Marchioli et al. (2010) expanded the parameter range and quantities examined in prior research, and investigated the rotation and orientation of prolate spheroids. They noted that prolate spheroidal particles, like spheres, tend to accumulate in the viscous sublayer, and both mean and fluctuating spin components of fibers depend crucially on the aspect ratio. Their studies also concluded that prolate spheroids are nearly randomly orientated in the central region, and have a preferential orientation in the streamwise direction in the near-wall region (Marchioli and

Soldati, 2013; L. Zhao et al., 2013b; Marchioli et al., 2016). Moreover, L. Zhao et al. (2012, 2014) further indicated that the preferential concentration dominates the relative translational motion between individual fibers and the surrounding fluid, and the particle inertia has a significant impact on fiber slip velocity. F. Zhao et al. (2013; 2015) studied fibers in wall turbulence using four-way coupling, and reported that the fluctuations of particle velocity are stronger than that of fluid velocity in the streamwise direction and significantly lower than of the fluid in the other directions in the near-wall region. It is also confirmed that large inertia prolate spheroids align parallel to local fluid vorticity in the central region (L. Zhao et al., 2015; Njobuenwu and Fairweather, 2016), and the Lagrangian fluid stretching direction in the nearly isotropic turbulence should be responsible for the distinct alignment (Pumir and Wilkinson, 2011; Ni et al., 2014; Chen et al., 2016; L. Zhao and Andersson, 2016).

On the other hand, knowledge about the dynamics of disk-like particles is far less complete than that of fiber-like particles. Njobuenwu and Fairweather (2013) found by means of large-eddy simulations (LESs) that both prolate and oblate spheroids segregate in the low-speed streaks. Challabotla et al. (2015c) reported that the translational motion of oblate spheroids has a weak dependence on the particle aspect ratio. Nevertheless, Challabotla et al. (2015c, b) also showed that the orientation and rotation of disks are qualitatively different from the dynamics of fibers. In the channel center, prolate are more likely to rotate around its symmetry axis (spin), whereas and oblate spheroids mostly rotate about the other two axes (tumble), and increasing inertia weakens the tendency of fibers to spin and disks to tumble (L. Zhao et al., 2015). Meanwhile, the near-wall preferential spanwise orientation of disk-like particles results in an alignment of the symmetry axis with the local vorticity vector (L. Zhao et al., 2015), which is ascribed to the direction of Lagrangian compression near the wall (L. Zhao and Andersson, 2016). Therefore, disk-like particles behave quite differently from fiber-like particles, and a further understanding of the translational and rotational motion of disks to unite the shape effect on the dynamics of spheroids is in demand.

Particularly, the presence of gravity is believed to be of practical importance in particle-laden turbulent flows. Uijttewaal and Oliemans (1996) reported that the gravity influences the distribution and deposition of spherical particles via the crossing trajectory mechanism. It has been indicated that there are more spheres concentrated at the channel center in a downward flow, and the drift of particles towards the walls increases in an upward flow (Marchioli et al., 2007; Nilsen et al., 2013). In addition, Zhang et al. (2001) observed that the deposition velocity of prolate spheroids in wall turbulence increases due to the presence of gravity in the flow direction. Siewert et al. (2014) explored the orientation and settling velocity over a wide range of particle shapes in decaying isotropic turbulence, and concluded that the preferential orientation and settling are induced by specific interactions of gravity and turbulence. Recently, Challabotla et al. (2016a, b) investigated the dynamics of fibers in turbulent vertical channel flows with three

different gravity configurations. They reported that the upward flow suppresses the drift velocity, and gives rises to a more uniform fiber distribution throughout the channel as compared to the distinct near-wall accumulation in the downward flow and in the absence of gravity.

The above-mentioned studies of disks suspended in turbulent flows show striking differences in the dynamics of disk-like and fiber-like particles. It is therefore likely that the influence of a gravity force on the dynamics of non-spherical particles will be different for disks than for fibers. In this paper, we perform a systematic study of gravity effects on the distribution, translation, rotation and orientation statistics of inertial disk-like particles modeled as oblate spheroids in vertical turbulent channel flow, aiming at improving the knowledge of disks and completely identifying the shape effect of spheroids as compared with the work by Marchioli et al. (2007) and Challabotla et al. (2016a, b). The oblate spheroids are characterized with shape and inertia parameterized by means of aspect ratio and Stokes number. Channel flows with opposing gravity, aiding gravity and in the absence of gravity have been considered. The rest of the present paper is organized as follows. In Section 2, the mathematical modeling related to the motion of both the fluid and particles are laid down. In Section 3, the effects of the gravity force on oblate spheroids distribution, translation, rotation and orientation are presented with the influence of particle shape and inertia. Finally, in Section 4, conclusions are drawn from the present study.

2.   Methodology

In the present work, an Eulerian-Lagrangian approach is adopted to investigate the dynamics of rigid oblate spheroidal particles dispersed in a turbulent vertical channel flow. Following the work by Marchioli et al. (2007) for spherical particles and Challabotla et al. (2016a, b) for prolate spheroidal particles, the three different gravity configurations with fluid flow in x direction are addressed, namely downward flow (GD), no-gravity flow (G0) and upward flow (GU), as illustrated in Fig. 1.
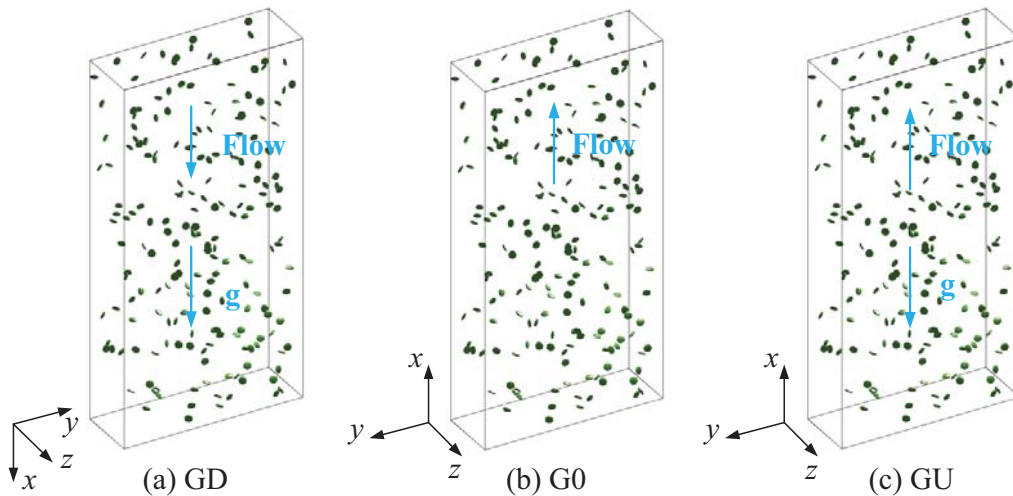
Fig. 1. Schematic representation of the problem: (a) downward flow; (b) no-gravity flow; (c) upward flow.

2.1. Eulerian fluid motion

The viscous fluid in which rigid disk-like particles are suspended is assumed to be incompressible, isothermal, and Newtonian. The continuity (mass conservation) equation and the Navier-Stokes (momentum conservation) equation can be expressed as,

$$\frac{\partial u_i}{\partial x_i} = 0,$$
(1)

$$\rho_f \left(\frac{\partial u_i}{\partial t} + u_j \frac{\partial u_i}{\partial x_j} \right) = -\frac{\partial p}{\partial x_i} + \mu \frac{\partial^2 u_i}{\partial x_j \partial x_j} + \underbrace{\left(-\frac{\partial P}{\partial x} \pm \rho_f g \right)}_{2\tau_w/h} \delta_{x,i},$$
(2)

where u_i is the component of the fluid velocity vector in the x_i direction and p is the fluctuating pressure, while ρ_f and μ denote the fluid density and dynamic viscosity, respectively. The body forces acting along the vertical channel include the negative mean pressure gradient $\partial P/\partial x$ and a negative or a positive gravity force $\rho_f g$. No-slip and impermeability boundary conditions on the fluid velocity are imposed at the channel walls whereas periodic boundary conditions are used in the homogeneous directions.

In all cases, the total driving force, i.e. the last term to the right in Eq. (2), is exactly balanced by the wall shear stress τ_w and h is the distance between the two parallel channel walls. The wall-friction velocity is defined as $u_\tau = \sqrt{\tau_w/\rho_f}$, and the frictional Reynolds number is $Re_\tau = u_\tau h/\upsilon$, in which the kinematic fluid viscosity $\upsilon = \mu/\rho_f$. The variables in Eqs. (1) and (2) can be normalized by the viscous scales for velocity u_τ, length (υ/u_τ) and time (υ/u_τ^2).

The direct numerical simulations of fluid flow are performed on a 6h×3h×h computational domain with 192×192×192 grid points in the streamwise (x), spanwise (y), and wall-normal (z) directions, respectively. The time-dependent three-dimensional turbulent flow field is obtained by integration of the fluid motion equations at Re_τ=360. The grid spacing in the wall-normal direction Δz^+ varies between 0.9 and 2.86 with a refinement towards both the channel walls, while the grid spacing in the two homogeneous directions are uniform with Δx^+=11.3 and Δy^+=5.6. The time step is Δt^+=0.036. The DNS solver used in the present study is the same as that employed by Gillissen et al. (2007), Mortensen et al. (2008b, a) and Challabotla et al. (2016a, b). The second-order finite-difference discretization is employed in the wall-normal direction, and the pseudo-spectral method is applied to the two homogenous streamwise and spanwise directions. The time advancement is carried out with a second-order explicit Adams-Bashforth scheme.

2.2. Lagrangian disk-like particles

A general rigid spheroidal particle is characterized by three semi-axes a, b, and c, in which $a = b$. The mathematical modelling of the dynamics of prolate spheroidal point particles (aspect ratio $\lambda = c/a > 1$) in wall turbulence has been outlined by Zhang et al. (2001), and subsequently adopted by Mortensen et al. (2008b, a) and Marchioli et al. (2010). In their work, two different

Cartesian coordinate systems are used. The translational motion is expressed in the inertial frame $x_i = (x, y, z)$, and the rotational motion is formulated in the particle frame $x_i' = (x', y', z')$ with its origin at the spheroid's mass center and the coordinate axes aligned with the symmetry axes of the spheroid.

Similarly, the translational motion of oblate spheroids ($\lambda = c/a < 1$) in the inertial frame also obeys Newton's second law,

$$m \frac{dv_i}{dt} = F_i \,, \tag{3}$$

where m is the particle mass; $v_i = (v_x, v_y, v_z) = dx_i/dt$ denotes the translational particle velocity in the inertial frame.

If the oblate spheroidal particle is sufficiently small, the neighboring flow can be considered as Stokesian, thus the force F_i acting on oblate spheroids can be expressed as,

$$F_i = \pi \mu a K_{ij} \Delta u_j \pm \left(1 - \frac{1}{D}\right) mg \delta_{x,i} \,, \tag{4}$$

where the positive and negative signs apply for downward (GD) and upward flow (GU), respectively, just as in Eq. (2). $D = \rho_p/\rho_f$ is the ratio between the particle density and fluid density. The resistance tensor K_{ij} is expressed in the inertial frame and related to the resistance tensor K_{ij}' in the particle reference frame as $K_{ij} = A_{ik}^t K_{kl}' A_{lj}$, where A_{ij} denotes the orthogonal transformation matrix which relates the same vector in the two different frames through the linear transformation $x_i' = A_{ij} x_j$.

The first term on the right-hand side of Eq. (4) represents the hydrodynamic drag force from the surrounding fluid on a non-spherical particle as derived by Brenner (1964). This expression for the drag force is valid only when the particle Reynolds number is sufficiently low such that the force acting on the particle is linearly dependent on the slip velocity Δu_i. Here, the slip velocity vector, defined as $\Delta u_j = u_{p,j} - v_j$, where $u_{p,j}$ is the fluid velocity seen by the particle along its trajectory and v_j is the particle translational velocity. The second term to the right in Eq. (4) accounts for gravity and buoyancy forces. The resistance tensor K_{ij}' is a diagonal matrix with elements obtained by Challabotla et al. (2015c),

$$K_{xx}' = K_{yy}' = \frac{32(1-\lambda^2)^{3/2}}{(3-2\lambda^2)C - 2\lambda(1-\lambda^2)^{1/2}}, \quad K_{zz}' = \frac{16(1-\lambda^2)^{3/2}}{(1-2\lambda^2)C + 2\lambda(1-\lambda^2)^{1/2}} \,, \tag{5}$$

where $C = \pi - 2\arctan(\lambda(1-\lambda^2)^{-1/2})$.

The rotational motion of oblate spheroids in the particle frame is given by Euler's equation,

$$I_{xx}' \frac{d\omega_x'}{dt} - \omega_y' \omega_z' (I_{yy}' - I_{zz}') = N_x',$$

$$I_{yy}' \frac{d\omega_y'}{dt} - \omega_z' \omega_x' (I_{zz}' - I_{xx}') = N_y', \tag{6}$$

$$I_{zz}' \frac{d\omega_z'}{dt} - \omega_x' \omega_y' (I_{xx}' - I_{yy}') = N_z',$$

where $I'_{xx}, I'_{yy}, I'_{zz}$ are the principal moments of inertia in the particle frame; $\omega'_x, \omega'_y, \omega'_z$ are the angular velocity of the spheroid in the particle frame. The torque components (N'_x, N'_y, N'_z) for a three-axial ellipsoidal particle in creeping shear flow were originally derived by Jeffery (1922). For oblate spheroids, the Jeffery equations can be simplified to:

$$N'_x = \frac{16\pi\mu a^3 \lambda}{3(\beta_0 + \lambda^2\gamma_0)}\left[(1-\lambda^2)S'_{yz} + (1+\lambda^2)(\Omega'_x - \omega'_x)\right],$$

$$N'_y = \frac{16\pi\mu a^3 \lambda}{3(\alpha_0 + \lambda^2\gamma_0)}\left[(\lambda^2-1)S'_{xz} + (1+\lambda^2)(\Omega'_y - \omega'_y)\right], \tag{7}$$

$$N'_z = \frac{32\pi\mu a^3 \lambda}{3(\alpha_0 + \beta_0)}(\Omega'_z - \omega'_z).$$

Here, S'_{ij} and Ω'_i denote the fluid rate-of-strain tensor and rate-of-rotation vector, respectively. These expressions are valid for any aspect ratio λ as long as the shape factors $(\alpha_0, \beta_0, \gamma_0)$ are defined as semi-infinite integrals. However, the analytical expressions for the shape factors for oblate spheroids due to Siewert et al. (2014),

$$\alpha_0 = \beta_0 = \frac{-\lambda^2}{1-\lambda^2} + \frac{\lambda C}{2(1-\lambda^2)^{3/2}}, \ \gamma_0 = \frac{2}{1-\lambda^2} - \frac{\lambda C}{(1-\lambda^2)^{3/2}}, \tag{8}$$

are different from the shape factors derived by Gallily and Cohen (1979) for prolate spheroids.

The ability of a disk-like particle to adjust to the ambient flow field can be estimated by the response time τ_p. As defined by Shapiro and Goldenberg (1993), a translational relaxation time based on the orientation-averaged resistance tensor $\overline{K} = 3(K'^{-1}_{xx} + K'^{-1}_{yy} + K'^{-1}_{zz})^{-1}$ is introduced. This is a relevant time scale for isotropically oriented particles and has been used by Mortensen et al. (2008a) and others for prolate spheroids. The same definition of an equivalent response time has also been adopted by Challabotla et al. (2015c) for the oblate spheroids,

$$\tau_p = \frac{4Da^2}{3\upsilon}\frac{\lambda}{\overline{K}} = \frac{\lambda C}{2(1-\lambda^2)^{1/2}}\frac{2Da^2}{9\upsilon}. \tag{9}$$

The Stokes number St is then defined as the ratio between τ_p and the viscous time scale υ/u_τ^2,

$$\text{St} = \frac{\tau_p u_\tau^2}{\upsilon}, \tag{10}$$

and the particle Reynolds number is defined as,

$$Re_p = \frac{d_{eq}<\Delta u_x>}{\upsilon}, \tag{11}$$

where $d_{eq} = a\lambda^{1/3}$ is the volume-equivalent diameter of the oblate spheroid and $<\Delta u_x>$ is the mean slip velocity in the streamwise direction.

There are totally 2×10^5 disk-like particles with semi major-axis $a^+ = 0.36$ of each type in our simulations. The particle suspensions are sufficiently dilute so that particle-particle collisions are rare and can be neglected. The spheroid-wall collisions are fully elastic, similar to the collision model used by Marchioli et al. (2010) and L. Zhao et al. (2014). Although the fluid motion might

be affected by the particles, especially in the near-wall region with relatively high particle concentrations (Li et al., 2001; L. Zhao et al., 2013a), the feedback from the disk-like particles onto the fluid is ignored in the present study. The effect of gravity on the dynamics of inertial disk-like particles in turbulent channel flow is explored by the one-way coupled simulations.

3.   Results and discussions

Simulations are performed for disk-like particles with Stokes numbers St=1, 5, 30, 100 and aspect ratios $\lambda = 0.1, 0.33, 0.999$ (see Table 1, in which some cases are retained to highlight trends only). The mathematical expressions for the resistance tensor K_{ij} in Eq. (5), the shape parameters α_0, β_0 and γ_0 in Eq. (8) and the response time τ_p in Eq. (9) exhibit singularities for $\lambda=1$. Particles with aspect ratio $\lambda=0.999$ are therefore considered as representatives of spherical particles. Combined with the three different gravity configurations depicted in Fig. 1, a total of $3 \times 3 \times 4$ different cases have been considered. In order to obtain reliable particle statistics, the present simulations have been run for a longer period of time than the earlier studies of fiber suspension flows (Challabotla et al., 2016a, b). The results are computed by averaging instantaneous data in the time window from $t^+ = 5400$ to 14400 and also in both the homogeneous streamwise and spanwise directions.

Table 1

The twelve different disk-like particle classes (constant semi major-axis $a^+=0.36$) with different mean and maximum particle Reynolds numbers Re_p.

Stokes number (St)	Aspect ratio (λ)	Density ratio (D)	Mean Re_p			Maximum Re_p		
			GD	G0	GU	GD	G0	GU
1	0.1	235	0.0112	0.0044	0.0101	0.0327	0.0217	0.0131
	0.33	80	0.0161	0.0063	0.0148	0.0469	0.0308	0.0187
	0.999	35	0.0235	0.0129	0.0236	0.0835	0.0639	0.0448
5	0.1	1175	0.0542	0.0212	0.0515	0.1481	0.0870	0.0753
	0.33	402	0.0774	0.0312	0.0733	0.2072	0.1350	0.1030
	0.999	174	0.0961	0.0505	0.1126	0.2963	0.1967	0.1671
30	0.1	7048	0.3120	0.0633	0.2960	0.6314	0.3014	0.3738
	0.33	2414	0.4625	0.0874	0.4230	0.9022	0.3977	0.5334
	0.999	1042	0.6446	0.1581	0.6145	1.2935	0.7126	0.8128
100	0.1	23492	0.9290	0.1731	0.9905	1.5724	0.6919	1.1432
	0.33	8046	1.4020	0.2502	1.4201	2.3969	0.9601	1.6768
	0.999	3472	2.1268	0.4553	1.8362	3.8077	2.0606	2.2813

As shown in Table 1, the mean and maximum particle Reynolds numbers, Re_p, in the streamwise direction increase with particle aspect ratio and Stokes number, and the mean Re_p is

relatively larger for the cases with gravity. The values of Re_p are almost consistently lower than unity, except for disk-like particles with the largest inertia (St=100). Although a few of the particle classes might be unrealizable, they are included here to make the test matrix complete. Therefore, the assumption of Stokes flow in the vicinity of the particles is otherwise reasonable, and the expressions for the viscous forces and torques can be justified.
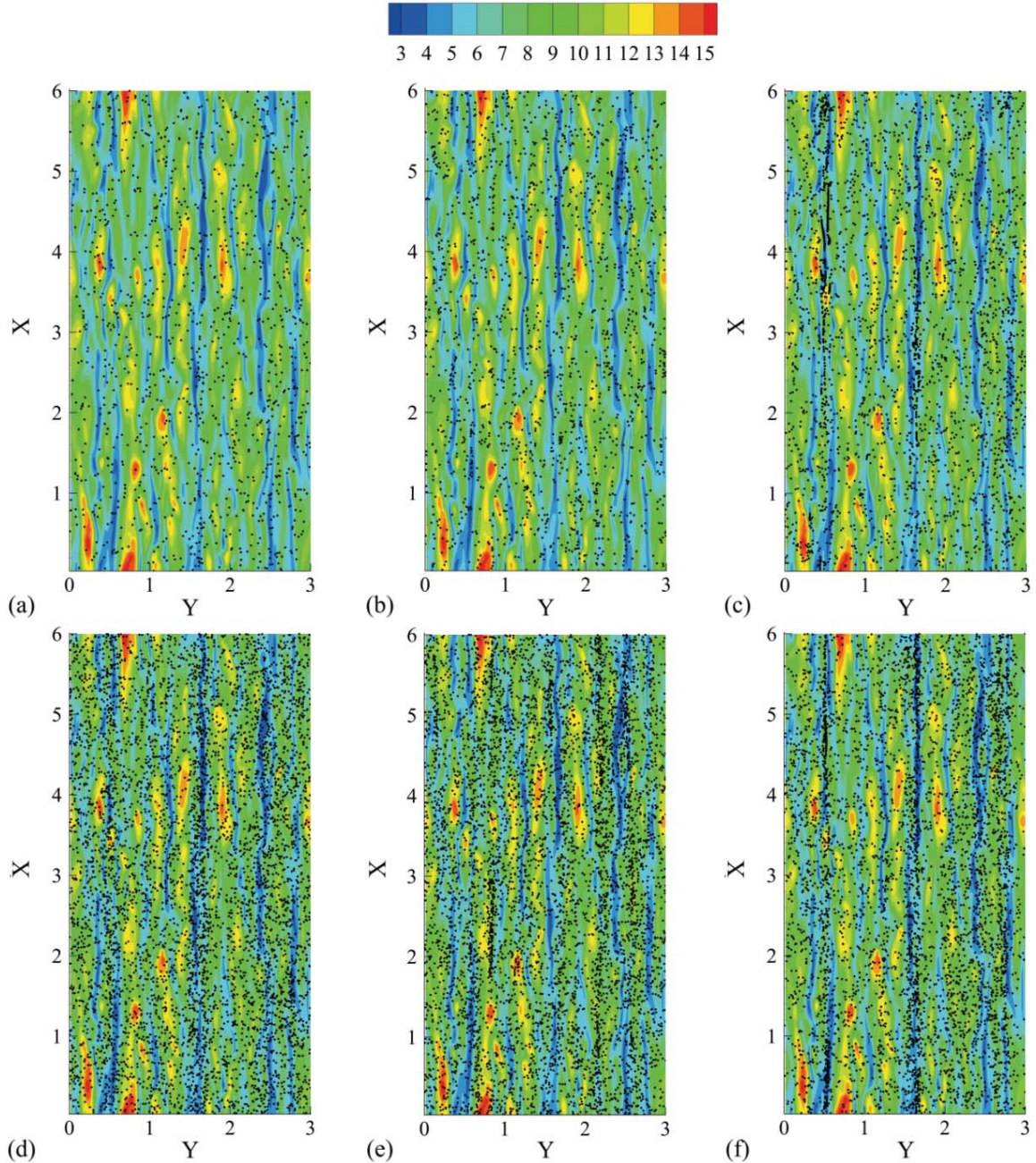
Fig. 2. Instantaneous distribution of disk-like particles with aspect ratio λ=0.33 for St=5 (upper row) and St=100 (lower row). (a) and (d) downward flow, (b) and (e) no-gravity flow, (c) and (f) upward flow. The disks are in the slab $7< z^+ < 9$ in buffer layer, and the colour contours in the background show the instantaneous streamwise fluid velocity.
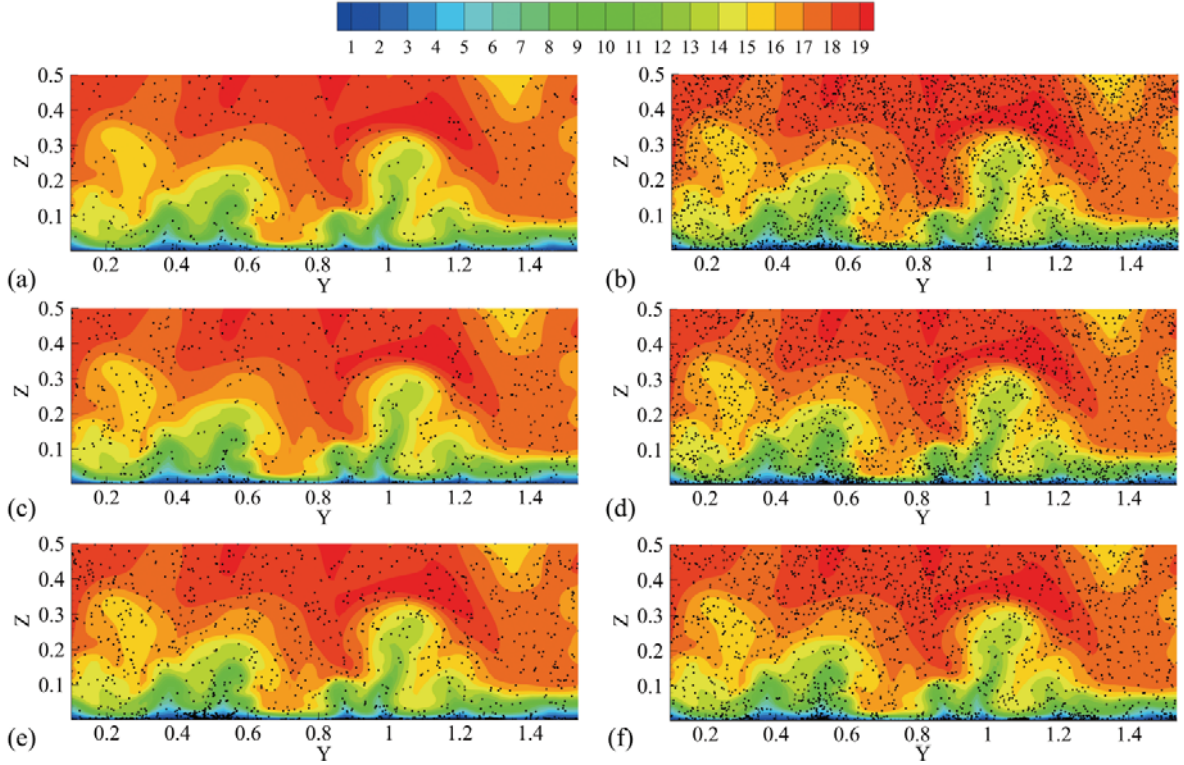
Fig. 3. Instantaneous distribution of disk-like particles with aspect ratio λ =0.33 for St=5 (left column) and St=100 (right column). (a) and (b) downward flow, (c) and (d) no-gravity flow, (e) and (f) upward flow. The colour contours in the background show the instantaneous streamwise fluid velocity. Only a quarter of the channel cross-section is presented.

The instantaneous distribution of disk-like particles with aspect ratio λ=0.33 are depicted in Figs. 2 and 3. The centers of mass of the disks are shown as black dots superimposed on the colour-coded streamwise velocity field in the background. However, due to the one-way coupled simulation and the constant total driving force, the velocity fields are all the same, regardless of the different gravity configurations.

In Fig. 2, the instantaneous disk distributions in the wall-parallel plane at $z^+ \approx$ 8 for St=5 (upper row) and 100 (lower row) are presented. Elongated red and blue fluid streaks characterize the high- and low-speed streaks in the buffer layer. It can be seen that disks at both Stokes numbers and irrespective of gravity preferentially cluster in low-speed streaks. Moreover, the instantaneous disk distributions in a quarter of the cross-sectional (y, z)-plane are shown in Fig. 3 for St=5 (left column) and St=100 (right column). Judging from Figs. 2 and 3, it is clear that the gravity force has a significant effect on the disk distribution across the channel and not only in the buffer layer. For St=5, we can observe a more even disk density across the channel in the upward flow as compared with the two other gravity configurations, while at St=100, this phenomenon is not obvious.

In the remaining sub-sections, we study the distribution, translation, rotation and orientation statistics of disk-like particles suspended in wall-bounded turbulence with different gravity

11

configurations. Although the simulations and the analyses have been carried out for four different Stokes numbers, in Section 3.1, we just present particle distributions and translations for St=5 and 100; while in Section 3.2, results for all four Stokes numbers are shown to discuss the rotational and orientational dynamics.

3.1. Distribution and translation
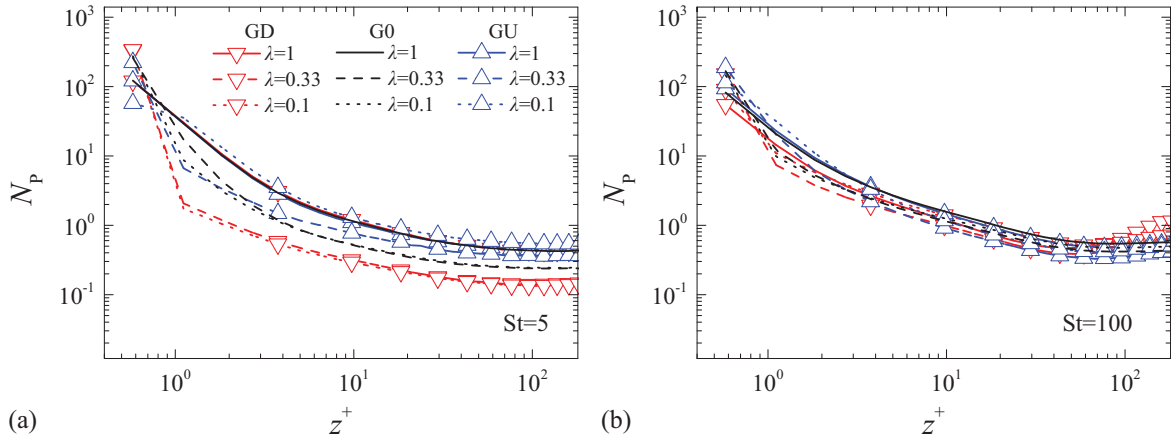
Fig. 4. Statistically averaged particle number density distribution over the half channel width for (a) St=5 and (b) St=100.

Fig. 4 shows the statistically averaged particle number density N_p from the wall to the channel center at z^+=180. The particle number is computed at different stages of the simulation with 100 bins in the wall-normal direction, and by counting the particle number in each bin all over the (x, y)-plane. The particle number density is normalized by the initial particle number distribution. For modest inertia (St=5), as shown in Fig. 4(a), the presence of gravity has a significant effect on the particle distribution and this influence is remarkably stronger for disk-like particles with larger asphericity (λ=0.1). In contrast, for large inertia (St=100), the distribution of disks is not so heavily influenced by the flow direction as that at St=5 (see Fig. 4(b)). The similar trend has also been observed in the work of Challabotla et al. (2016b) for fibers, indicating that the effects of gravity and shape on spheroid distribution always reduce with the increase of inertia.

Inertial particles are drifting with relatively high streamwise momentum from the central region towards the near-wall region and accumulate in low-speed streaks in the wall vicinity (Balachandar, 2009; Soldati and Marchioli, 2009). This phenomenon occurs for inertial fibers (Marchioli et al., 2010) and disks (Challabotla et al., 2015c) as well. However, except for the concentration in the near-wall region, it is observed that disk-like particles also have a tendency of gathering in the central region with increasing inertia. This trend is apparent for high-Stokes-number spheroids in the downward flow, and accords with previous results reported by Marchioli et al. (2007) and Challabotla et al. (2016b). Interestingly, the phenomenon that the upward flow

leads to a more uniform fiber distribution (Challabotla et al., 2016b) is not obvious in the present work. The differences between the disk distributions in the three gravity configurations are believed to influence other statistical characteristics, such as the mean and fluctuating particle velocity components and the rotational dynamics. Such alterations will be considered in the following.
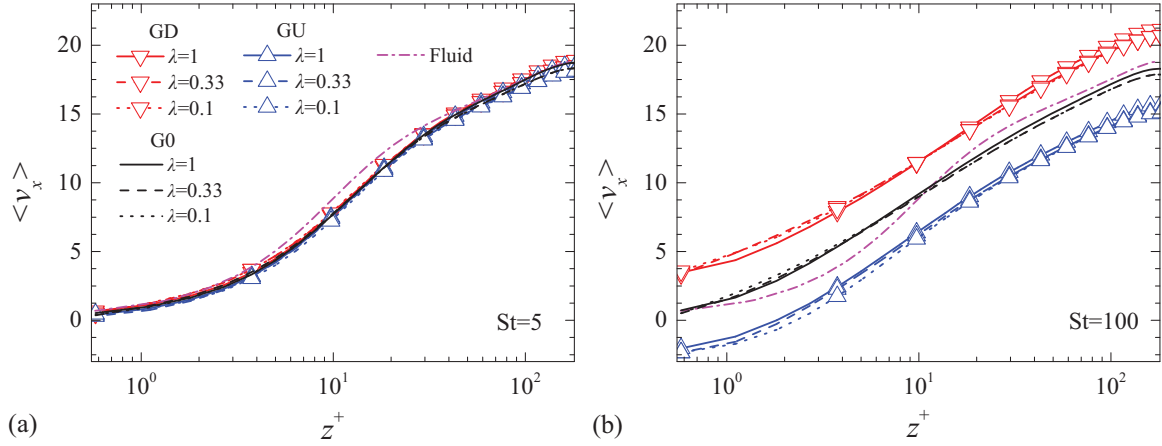
Fig. 5. Mean streamwise particle velocity $<v_x>$ and Eulerian fluid velocity $<u_x>$ for (a) St=5 and (b) St=100.

The mean streamwise particle velocity $<v_x>$ and the Eulerian fluid velocity $<u_x>$ are shown as a function of the wall-normal coordinate z^+ in the semi-logarithmic plots in Fig. 5. Clearly, the effect of spheroid shape on the mean velocity is practically negligible in the whole channel, which is in close agreement with the results reported by Challabotla et al. (2016b) for fibers. For modest inertia (St=5), the mean particle streamwise velocity is almost unaffected by the presence of gravity. However, for large inertia (St=100), the influence of gravity force becomes important, and the inertial disk-like particles distinctly lead the fluid in the downward flow and lag behind the fluid in the upward flow. Similar trends have also been reported for spheres by Marchioli et al. (2007) and for fibers by Challabotla et al. (2016b). Therefore, the gravity force is strongly correlated with the particle slip velocity for large inertia particles. Besides, for St=100, the mean particle velocity is positive for the downward flow and negative for the upward flow in the near-wall regions, which is different from the translational motion of fibers near the wall described by Challabotla et al. (2016b). It can be inferred that, in the upward flow, though spheroids in the channel center move in the streamwise direction, the large inertia drives the oblate spheroids to sink near the wall. This is mainly because a disk-like particle away from the center suffers a smaller drag force than the inertial fiber, and fibers and disks may moreover have different angles of attack near the wall.

13
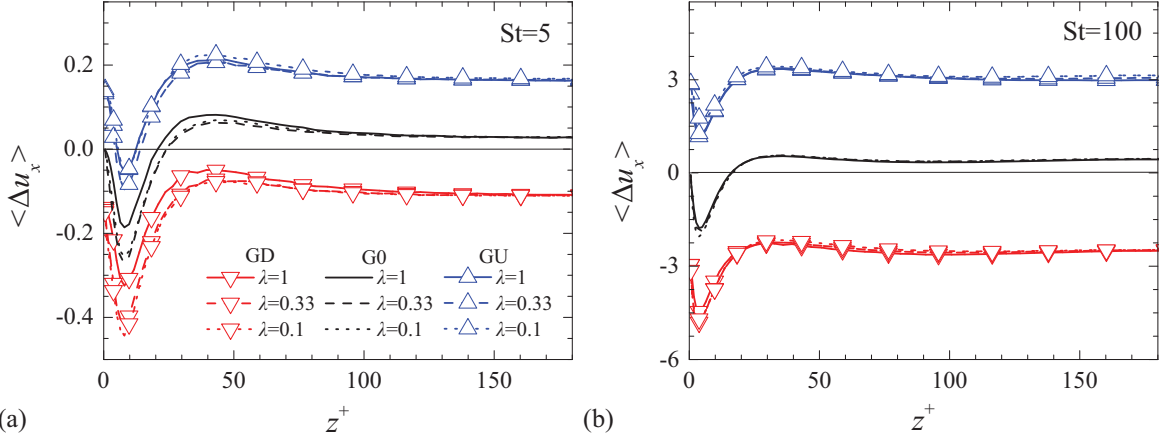
Fig. 6. Mean streamwise particle slip velocity $\langle\Delta u_x\rangle$ for (a) St=5 and (b) St=100. Notice the scaling of vertical axis in the different panels.

The mean streamwise slip velocity $\langle\Delta u_x\rangle$, defined as $\langle u_{p,x}\rangle - \langle v_x\rangle$, is presented in Fig. 6 as a function of the wall-normal coordinate z^+. It is remarkable that the channel wall has a significant impact on the streamwise slip velocity of disk-like particles, and the value of $\langle\Delta u_x\rangle$ rises with the increasing inertia. However, the particle shape plays little role on $\langle\Delta u_x\rangle$ in the center region, although a modest shape-dependence is observed around $z^+=10$ for St=5. These findings also accord well with the observations for fibers by Challabotla et al. (2016b), suggesting that the spheroid shape almost has only negligible influence on the particle slip velocity.

In the absence of gravity (G0), $\langle\Delta u_x\rangle$ is negative in the near-wall region and positive in the rest of the channel, which is similar to the results for fibers reported by Mortensen et al. (2008b) and L. Zhao et al. (2014). This implies that spheroids lead the fluid near the wall and lag behind the fluid in the core region. Moreover, larger streamwise slip velocities are observed in the presence of gravity. In the downward flow (GD), $\langle\Delta u_x\rangle$ is negative throughout the entire channel. The disk-like particles in the viscous sublayer experience a negative viscous drag force in this case, which gives rise to a large migration velocity in the streamwise direction. On the contrary, in the upward flow (GU), the negative drag persists only in the near-wall region when $\langle\Delta u_x\rangle$ remains negative for St= 5, and the mean slip is consistently positive even in the wall vicinity for St=100. The viscous fluid therefore tends to drag oblate spheroids in the positive upward direction, and the Stokes drag opposes the gravity force in these cases.

14
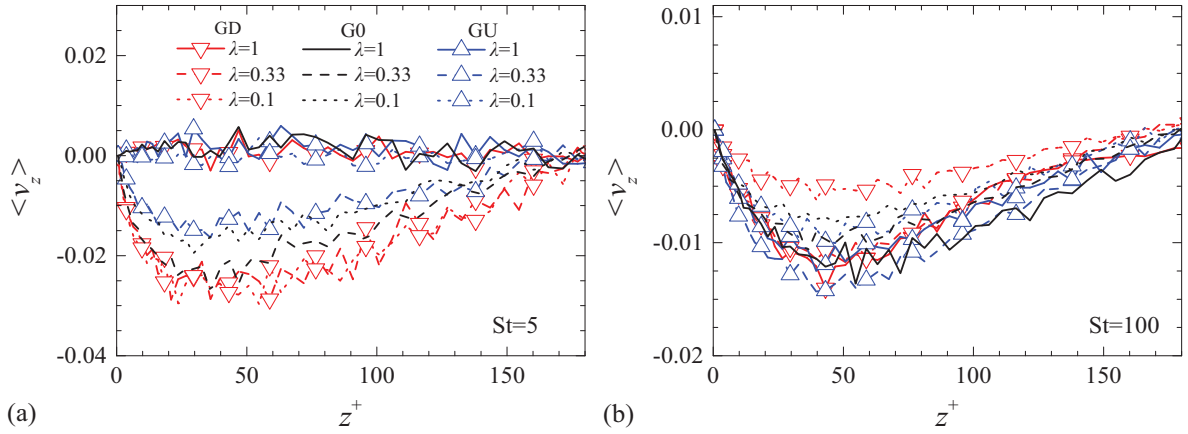
Fig. 7. Mean wall-normal particle velocity $\langle v_z \rangle$ for (a) St=5 and (b) St=100.

The mean wall-normal velocity $\langle v_z \rangle$ of disk-like particles, namely the drift velocity, referring to the lateral migration, has a close relation with the final distribution of disks and is worthwhile a discussion. As shown in Fig. 7, the mean wall-normal disk velocity $\langle v_z \rangle$ varies with the wall-normal coordinate z^+. The essentially negative value of $\langle v_z \rangle$ shows that disk-like particles are moving away from the center and towards the walls, and have not yet reached a statistically-steady state. It can be observed that $\langle v_z \rangle$ decreases with the growing Stokes number, and the maximum value of $\langle v_z \rangle$ is around $z^+ \approx 40$. Compared with the results of fibers by Challabotla et al. (2016b), this phenomenon occurs at the same place.

For St=5 (Fig. 7(a)), smaller drift velocities are observed for disk-like particles in the upward flow, while the flattest spheroids (λ=0.1) have the largest $\langle v_z \rangle$ in the downward flow. They are in a statistically-steady state in the upward flow similarly to spheres unaffected by gravity. In addition, for St=100 (Fig. 7(b)), disk-like particles with a smaller aspect ratio invariably have a slower normal-wall motion in a given flow configuration, and the downflow triggers a smaller drift velocity for oblate spheroids. These observations are qualitatively different from the performance of fibers (Challabotla et al., 2016b), and the near-wall orientation of disk-like particles is believed to play an important role here. Frankly, it is hard to sum up a distinct trend for the normal-wall movement of spheroids associated with the effects of particle shape and inertia. However, the negative mean drift velocities provide evidence that the overall movement of oblate spheroids is directed towards the channel walls, reflecting the higher number of particles in the near-wall region shown in Fig. 4.
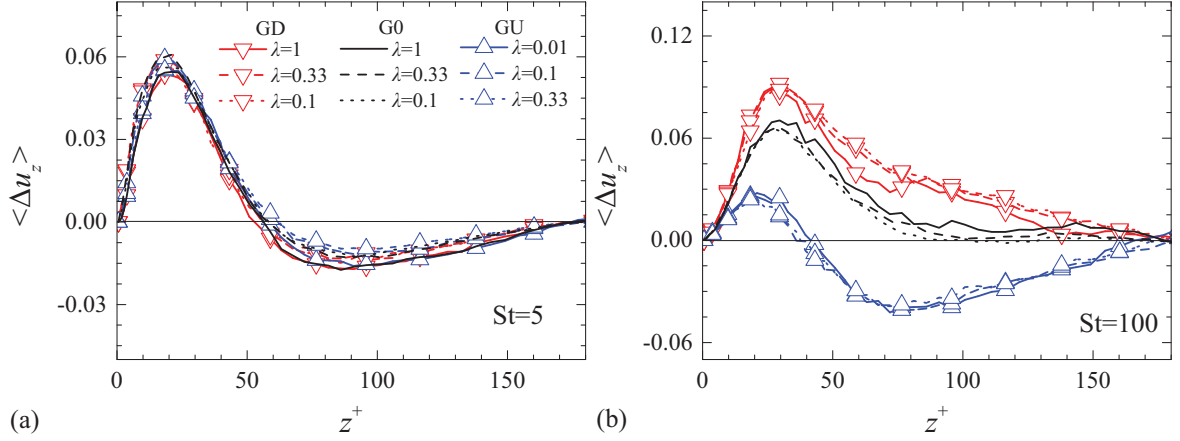
Fig. 8. Mean wall-normal particle slip velocity $\langle\Delta u_z\rangle$ for (a) St=5 and (b) St=100.

As shown in Fig. 8, the mean slip velocity in the wall-normal direction $\langle\Delta u_z\rangle$ presents no discernible dependence on the spheroid shape, just as that in the streamwise direction. For St=5, the wall-normal slip velocities of spheres as well as disks are nearly unaffected by the flow direction (Fig. 8(a)). In these cases, $\langle\Delta u_z\rangle$ exhibits a major non-monotonic dependence on the distance to the wall, which increases in a limited range and drops to zero at $z^+\approx50$. The largest positive slip velocity is found at $z^+\approx20$, suggesting that ejection events are dominating the disk-like particle transport towards the channel center (this finding agrees well with the work by Challabotla et al. (2016b)). Besides that, the mean wall-normal slip velocity is invariably negative further away from the wall and eventually returns to zero in the channel center, indicating that disk-like particles suffer an inertial lift towards the channel wall.

Furthermore, $\langle\Delta u_z\rangle$ rises with inertia. The trends reported by L. Zhao et al. (2012) for fibers without gravity and by Challabotla et al. (2016b) for fibers with gravity have been reproduced. For St=100, the gravity significantly influences the mean wall-normal slip velocity (Fig. 8(b)). In the downflow configuration (GD), $\langle\Delta u_z\rangle$ is invariably positive, indicating that disks as well as spheres experience a positive force towards the channel center and are likely to form a localized concentration in the central region. It can be confirmed by revisiting Fig. 4(b) that there are more disk-like particles in the channel center in the downward flow. Analogously, in the upward flow (GU), for the negative $\langle\Delta u_z\rangle$ in the central region, the force on disk-like particles results in a denser distribution near the channel wall. Particularly, in the absence of gravity (G0), oblate spheroids near the channel center with zero wall-normal slip velocity have an intermediate particle distribution relative to the cases with gravity. Nevertheless, $\langle\Delta u_z\rangle$ in the near-wall region obviously rises more quickly in the downward flow at St=100. The largest $\langle\Delta u_z\rangle$ therefore occurs in the downward flow whereas the lowest slip velocity is found in the upward flow.

As revealed in Fig. 7, due to the negative mean drift velocities, the overall tendency of disk-like particles is their movement towards the channel walls. Therefore, the positive $\langle\Delta u_z\rangle$ in Fig. 8(b) mainly arises from three different reasons: (1) $v_z < u_{p,z} < 0$; (2) $v_z < 0 < u_{p,z}$; (3) $0 < v_z < u_{p,z}$.

16

Disk-like particles in the central region move faster towards the wall by means of sweeps in the upward flow, i.e. case (1). On the other hand, in the near-wall region, the fluid is undoubtedly ejected away from the wall, and oblate spheroids can migrate to the wall and be pushed back, i.e. case (2) and (3). In general, the flow configuration has no impact on the fluid flow and the feedback from disk-like particles onto the fluid is also ignored in our simulations. By revisiting Figs. 7 and 8, one can infer that the gravity force alters the particle position in the flow field. The inertia disk-like particles are more likely to locate in inward fluid excursions ($u_{p,z} < 0$) in the upward flow and in outward fluid excursions ($u_{p,z} > 0$) in the downward flow.

These findings can also be explained by the presence of turbophoresis, i.e. the tendency that inertial particles move towards regions of lower turbulence intensity (Marchioli and Soldati, 2002). In the upward flow, the gravity attenuates this tendency as particles are likely to locate at higher-speed fluid regions, so that the distribution of oblate spheroids is more uniform across the channel width. In contrast, this tendency in stronger in the case of downward flow, in which the particles seem to move to lower-speed fluid regions, resluting in a denser concentration both in the central and the near-wall regions. This subtle effect of gravity varies with the inertia and the shape of the oblate spheroids. The large inertia reduces this tendency and the particle mass as well as the near-wall rotation along with different aspect ratios make this problem more complex.
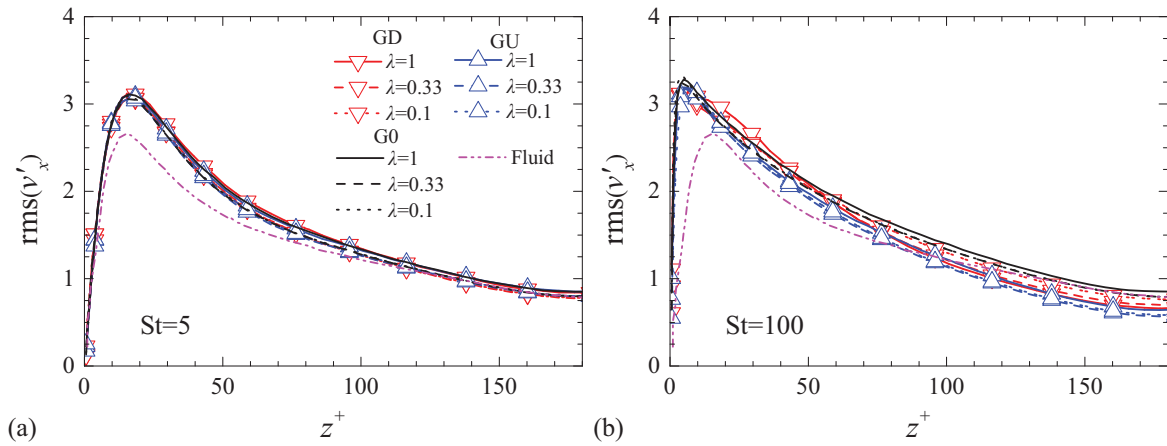
Fig. 9. rms-values of streamwise particle velocity fluctuation (rms(v'_x)) and Eulerian fluid velocity fluctuation (rms(u'_x)) for (a) St=5 and (b) St=100.

In the turbulent channel flow, the disk velocities are no doubt fluctuating about their mean values similarly as the fluid velocities. Root-mean-square (rms) values of the streamwise and wall-normal velocity components of disk-like particles and Eulerian fluid are shown in Figs. 9 and 10, respectively. The particle velocity fluctuations exceed the corresponding Eulerian fluid velocity fluctuations in the streamwise direction, as shown in Fig. 9; whereas rms(v'_z) is smaller than rms(u'_z) all the way from the wall to the center, as shown in Fig. 10.

For modest inertia (St=5), the influence of spheroid shape on the particle intensities is

negligible, which is in accordance with the previous results of fibers without gravity (Mortensen et al., 2008b) and with gravity (Challabotla et al., 2016b). The rms profiles for different gravity configurations are overlapping, implying that the gravity force, together with the spheroid shape, have negligible effects on the velocity fluctuations. On the contrary, for large inertia (St=100), oblate spheroids behave rather differently. The streamwise fluctuations exceed the fluid fluctuations in the near-wall region and approach rms(u'_x) in the channel center (Fig. 9(b)); while the wall-normal fluctuations seem to decline with the increasing inertia, and the peak of rms(v'_z) at $z^+ \approx 50$ eventually disappears for the large inertia (Fig. 10(b). Furthermore, wall-normal fluctuations for high-Stokes-number particles are substantially reduced in comparison with the corresponding fluid velocity fluctuation (Fig. 10(b)). The no-gravity configuration appears to have a slightly stronger particle velocity fluctuations in the channel center for this large inertia case. Though the downward flow slightly augments the streamwise velocity fluctuation and attenuates the wall-normal velocity fluctuations in the channel center, the effects of gravity force as well as particle shape are of modest significance. The velocity fluctuations of disk-like particles can be primarily ascribed to particle inertia.
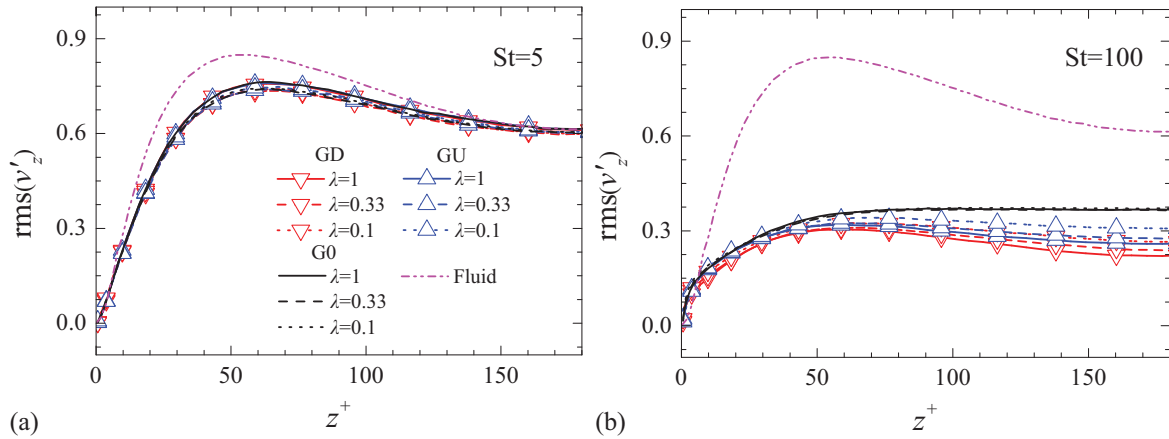
Fig. 10. rms-values of wall-normal particle velocity fluctuation (rms(v'_z)) and Eulerian fluid velocity fluctuation (rms(u'_z)) for (a) St=5 and (b) St=100.

3.2. Rotation and orientation
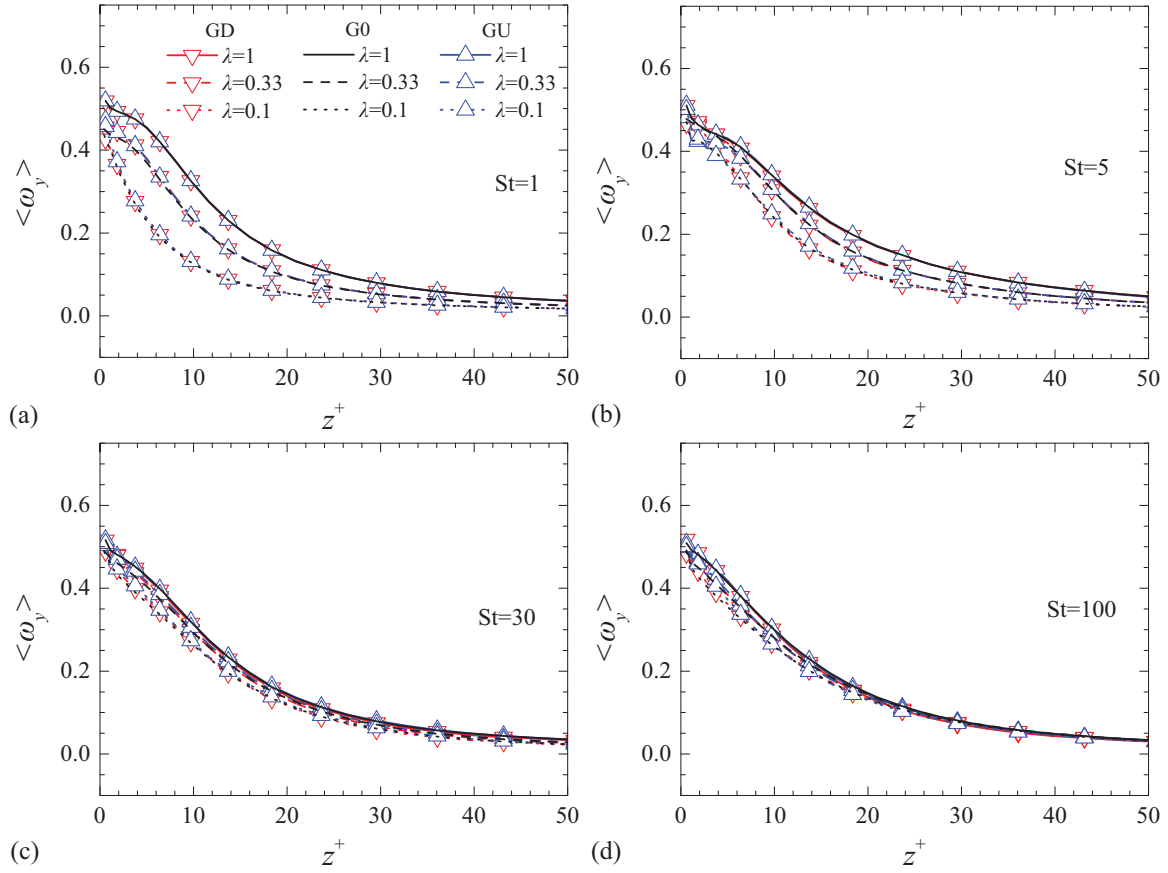
Fig. 11. Mean spanwise angular velocity in the near wall region for (a) St =1; (b) St =5; (c) St = 30 and (d) St = 100.

Though the mean particle angular velocities in the streamwise and wall-normal directions are zero, the mean spanwise value $<\omega_y>$ in the near-wall region is shown in Fig. 11. Clearly, the presence of gravity has a negligible influence on the mean angular velocity, regardless of the particle inertia and shape. Spheres as well as disks are inclined to spin near the wall, and the particles prefer to be irrotational near the channel center. In particular, disk-like particles with higher aspect ratio λ have a larger angular velocity near the channel wall. This trend is consistent with the results reported by Challabotla et al. (2015c) for disk-like particles in the absence of gravity, but quite different from the rotational statistics of fibers reported (Mortensen et al., 2008b; Marchioli et al., 2010; Challabotla et al., 2016a), that the mean spanwise fiber spin in the near-wall region decreases with increasing aspect ratio λ. These results mean that both elongated fibers and flat disks hardly obtain a high angular velocity in the near-wall region.
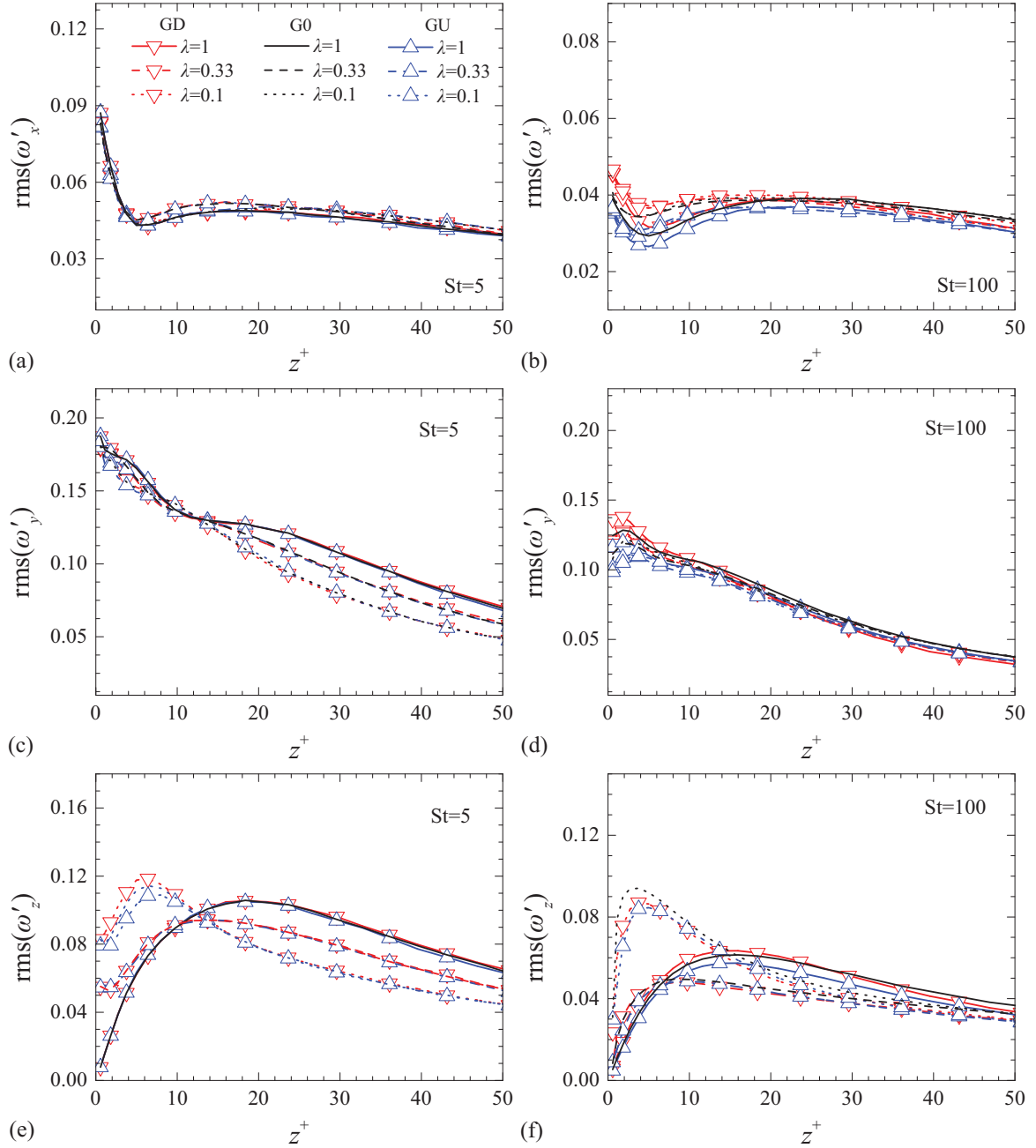
Fig. 12. rms-values of the angular velocity fluctuations in different directions for (a-c-e) St=5 and (b-d–f) St=100. (a, b) streamwise direction; (c, d) spanwise direction; (e, f) wall-normal direction.

The three rms components of the angular velocity fluctuations are shown in Fig. 12 for St=5 (left column) and St=100 (right column). It is noted that disk-like particles possess fairly strong spin fluctuations in the streamwise and wall-normal directions, in spite of the fact that mean spin components about the streamwise and the wall-normal axes are zero. Furthermore, the spin fluctuations next to the wall are distinctly larger for St=5 than that for St=100, whereas the gravity effect is always modest and confined to a region very close to the wall. In particular, the

spin fluctuations are distinctly anisotropic with the highest and lowest levels in the spanwise and streamwise directions, respectively. This reflects the prevailing anisotropy of the vorticity fluctuations in the buffer region. However, the intensity of spin fluctuations then decreases with increasing distance from the wall, and eventually tends towards isotropy in the core region.

Nevertheless, similar to $<\omega_y>$ in Fig. 11, the spheroid shape has a strong influence on the angular velocity fluctuations, but this shape effect gradually vanishes with the increasing inertia. Both rms(ω_y) and rms(ω_z) are seen to increase with the increasing λ beyond $z^+ \approx 15$. In the near-wall turbulence, however, the flattest spheroids obviously exhibit a stronger wall-normal spin fluctuation. These observations can be viewed in combination with the results for fibers by Challabotla et al. (2016a). By revisiting Eq. (7), the viscous torques are contributed by the fluid strain and the fluid rotation, and always strive to make the particles rotate along with the local vorticity. The observed particle spin is accordingly a signature of the local flow field and, in particular, of the fluid rotation in the vicinity of the particles. Therefore, the rotational performance of fibers and disks implies that spheroids with greater departure from sphericity are hard to rotate with the fluid vorticity in the central region, and both elongated fibers and flat disks are sensitive to the near-wall fluctuating fluid. This is due to the particle moment of inertia, which makes the rotational response time of an individual spheroid strongly dependent on the aspect ratio (Challabotla et al., 2015c).

(a)   (b)   (c)   (d)
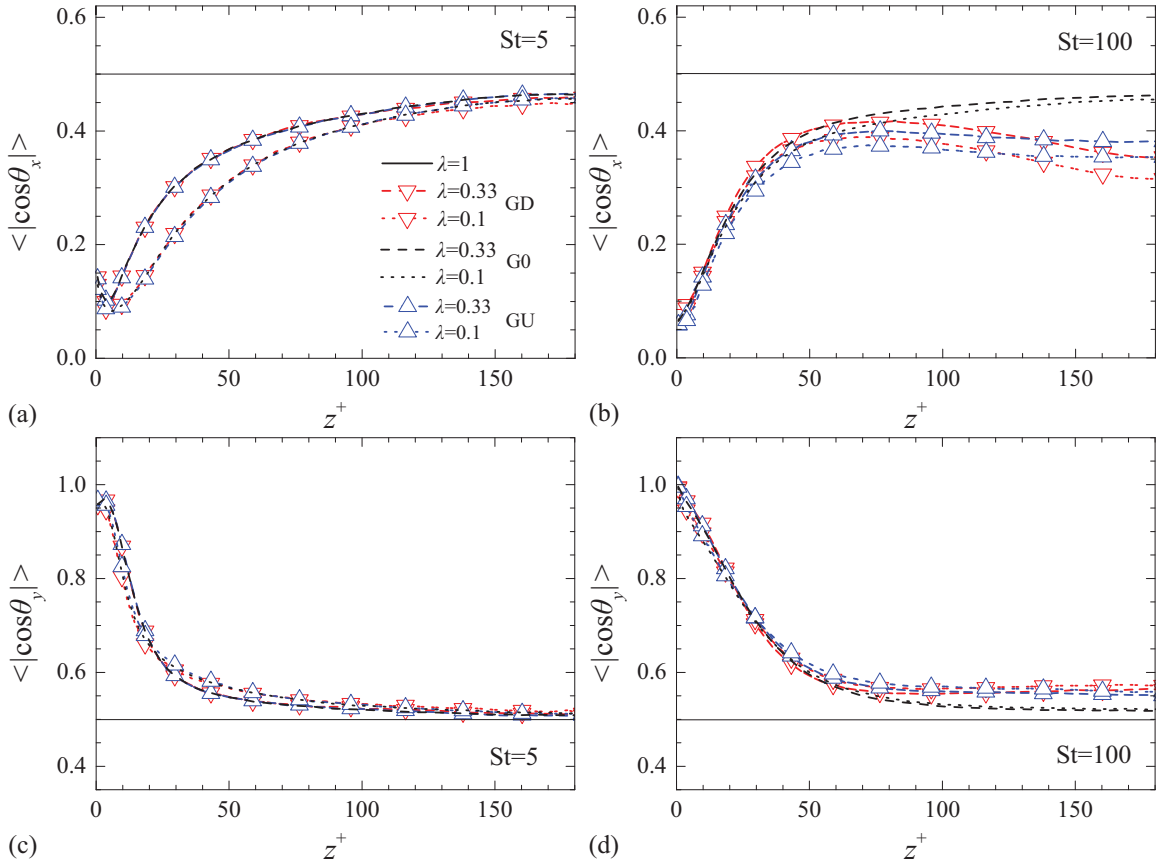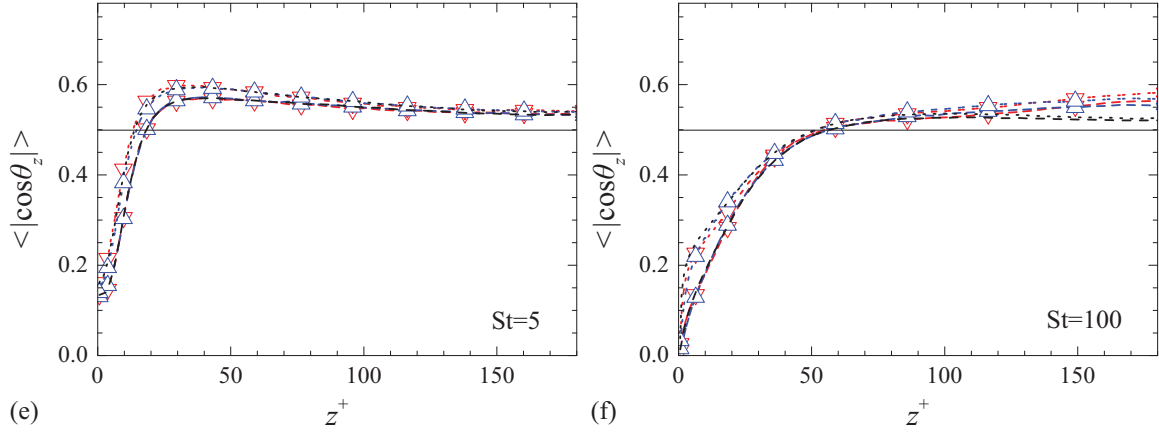
Fig. 13. Mean absolute cosines of the angle between the disk's symmetry axis for (a-c-e) St=5 and (b-d–f) St=100. (a, b) streamwise direction; (c, d) spanwise direction; (e, f) wall-normal direction.

The mean absolute direction cosines depend on the shape of disk-like particles and gravity force as presented in Fig. 13, with modest inertia (St=5) to the left and for large inertia (St=100) to the right. Here, the orientation of an oblate spheroid is measured as $<|\cos(\theta_i)|>$, referred to as direction cosine, and defined in terms of the angle θ_i between the symmetry axis of the spheroid and the x_i-axis of the inertial frame. It is found that the presence of gravity has a negligible impact on the orientation of disk-like particles, regardless of the disk inertia and shape. Moreover, the mean absolute direction cosines in the channel center are $<|\cos(\theta_x)|> \approx <|\cos(\theta_y)|> \approx <|\cos(\theta_z)|> \approx 0.5$, reflecting a random orientation of disk-like particles. This observation is coincident with the performance of inertial fibers (Mortensen et al., 2008a; Marchioli et al., 2010; Challabotla et al., 2016b). In the near-wall region, however, the preferential orientation is in the spanwise y-direction, i.e. $<|\cos(\theta_y)|> \approx 1$. This is at variance with the observation of fibers near the wall (Mortensen et al., 2008a; Marchioli et al., 2010; Challabotla et al., 2016b), that elongated fibers tend to align in the streamwise direction in the wall region, but is consistent with our recent finding that a single inertial disk-like particle in uniform shear flow ultimately tends to rotate in the flow-gradient plane (Challabotla et al., 2015a). Thus, a common feature of disks and fibers in the near-wall region is that both tend to align their long axis in the mean-shear plane.

In addition, for modest inertia (St=5), it is observed that the preferential orientation of disk-like particles is shape-dependent in the vicinity of the wall ($z^+ \leq 50$), and the flattest spheroids (λ=0.1) also have a tendency to orientate in the wall-normal direction (this is more apparent at St=1, but not reported). While with increasing inertia (St=100), the preferential orientation is firmly in the spanwise rather than in the wall-normal direction. This change of the preferred disk orientation occurs when inertia becomes more influential than shape.

It is of particular interest that the mean absolute direction cosines departure from 0.5 (i.e. isotropy) in the channel center with the presence of gravity. This is similar to the observation for fibers (Challabotla et al., 2016b), indicating that spheroids are less likely to orient randomly in

the central region when the flow is either upward or downward. The negligible effect of gravity on the absolute cosines in the near-wall region moreover suggests that Lagrangian compression and not gravity dominates the preferential orientation of disk-like particles in wall turbulence (L. Zhao and Andersson, 2016).
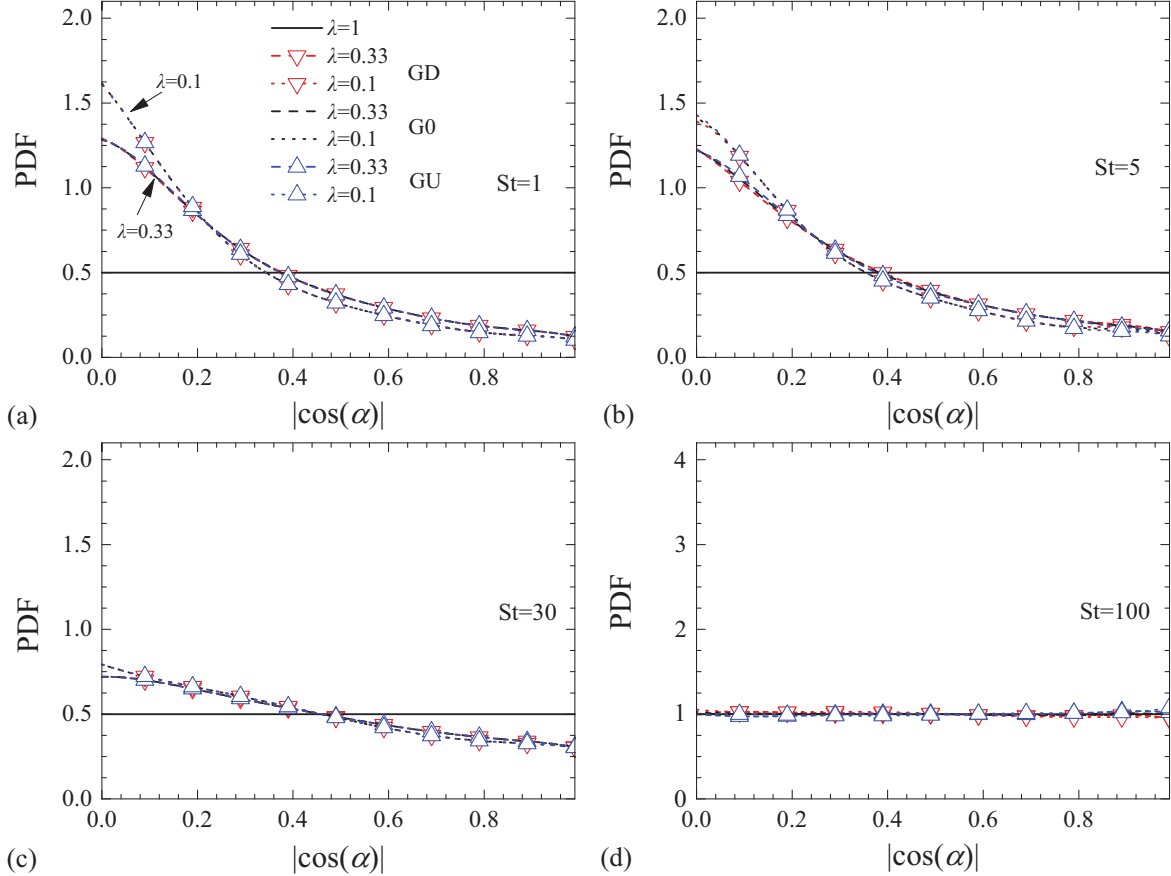
Fig. 14. Channel-center (at $z^+= 180$) distributions of particles' instantaneous alignment α with the local fluid vorticity for (a) St =1; (b) St =5; (c) St = 30 and (d) St = 100.

In order to unite the disparate orientations of disk-like particles from the channel center to the near-wall region, probability density functions of the absolute direction cosine of spheroid instantaneous alignment α (the angle between the spheroid's symmetry axis and the local fluid vorticity vector), PDF($|\cos(\alpha)|$), are presented in Figs. 14 and 15. Obviously, the presence of gravity has a negligible impact on the preferential alignment of disk-like particles, in consistence with the results for oblate particles' rotation and orientation in Figs. 11, 12 and 13. On the other hand, according to Fig. 14, disk-like particles tend to align with their symmetry axis (z') orthogonal to the fluid vorticity in the nearly isotropic channel center. This tendency would be attenuated with increasing inertia, eventually leading to a random alignment in the channel center for St=100 (Fig. 14(d)). This also replicates previous observations for non-inertial oblate spheroids in homogeneous isotropic turbulence (Gustavsson et al., 2014; Marcus et al., 2014;

Byron et al., 2015).

By comparing corresponding lines between λ=0.33 and λ=0.1 at modest inertia, the preferential alignment of spheroid's long axis in the direction of fluid vorticity vector becomes slightly stronger for disks with greater departure from sphericity. This is consist with the results of L. Zhao et al. (2015) and Njobuenwu and Fairweather (2016) that the alignment effect of spheroids becomes slightly stronger for particles with greater departure from sphericity, although the focus of their work is on the alignment of rod-like particles parallel to the local fluid vorticity in the channel center. In addition, increased particle inertia weakens the alignment effect for all particle shapes, making the orientation of disk-like particles more isotropic in the channel center.
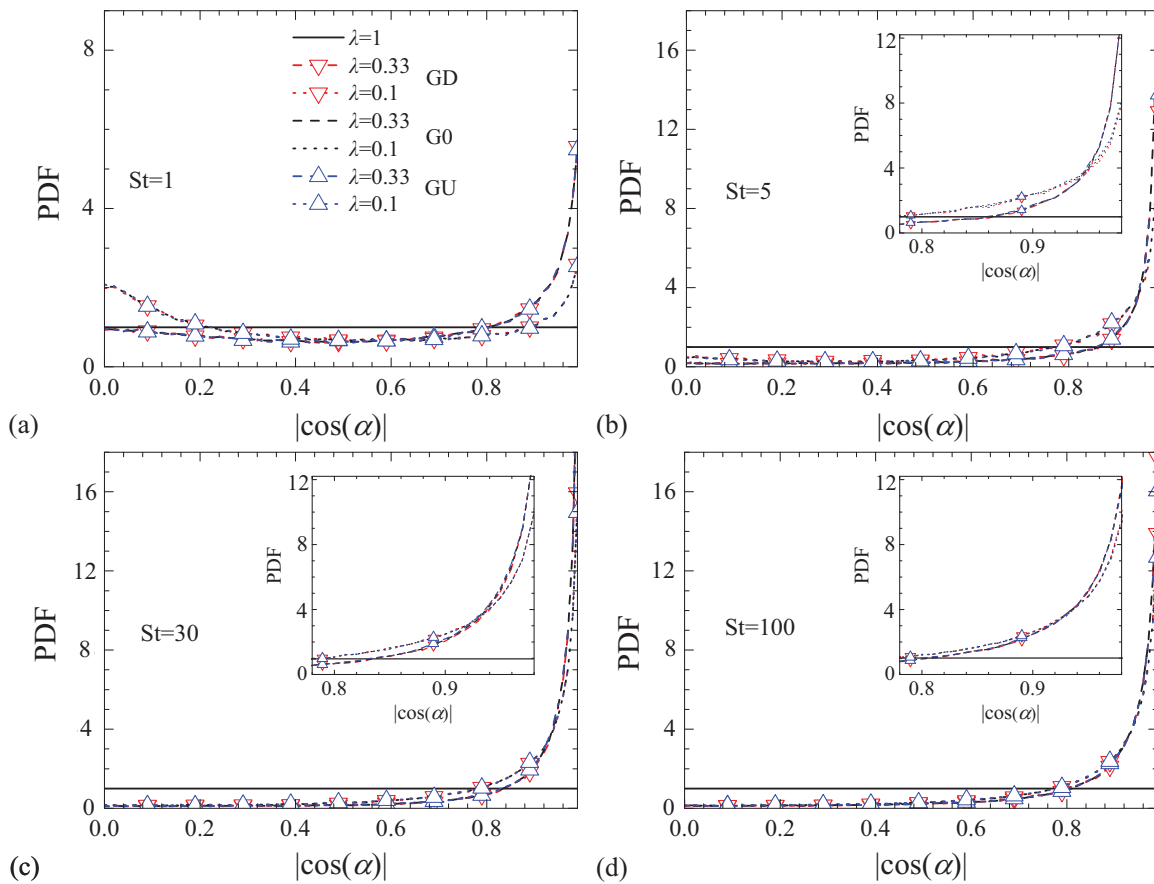
Fig. 15. Near-wall (at z^+= 10) distributions of particles' instantaneous alignment α with the local fluid vorticity for (a) St =1; (b) St =5; (c) St = 30 and (d) St = 100.

Unlike in the channel center, as shown in Fig. 15, near-wall disk-like particles prefer parallel alignment relative to the fluid vorticity when the inertia is increased. This type of preferential alignment is controlled by particle inertia, and is almost independent of particle shape for large inertia (St=30 and 100). This result conforms with the observation by L. Zhao et al. (2015) for disks without gravity. However, the flattest spheroids are less likely to orient parallel to the fluid vorticity for modest inertia (St=1), and even have a tendency to align perpendicularly ($|\cos(\alpha)\approx 0|$).

As suggested by Voth (2015) and L. Zhao et al. (2015), the preferential alignment of disk-like particles with modest inertia can be simply explained by considering Jeffery orbiting in the mean shear, while the alignment of high-Stokes-number disks is controlled by particle inertia. By revisiting the rotation statistics in Fig. 11 and the preferential orientations in Fig. 13, it can be concluded that, in the near-wall region, heavy disk-like particles with large inertia have a mean rotation that is almost equal to the mean fluid rotation, while light spheroids with modest inertia have a lower rotation rate that decreases with larger asphericity.

In general, the preferential alignment seen near the wall is more significant and is opposite to that at the channel center, suggesting that different mechanisms dominate particle orientation. The Lagrangian coherent structures (LCSs) (Haller, 2015) acting as organizers of transport in turbulent flows have a clear impact on the particle trajectory, and should be responsible for the distinct alignment of disk-like particles. A possible explanation for the preferential alignment is suggested by recent findings, that the symmetry axis of prolate spheroids align with the direction of strongest Lagrangian stretching whereas oblate spheroids orient with the direction of Lagrangian compression (Ni et al., 2014; L. Zhao and Andersson, 2016).

4.   Conclusions

This work has investigated the dynamic behavior of inertial disk-like particles in turbulent vertical channel flow. The turbulent flow field is obtained by means of a direct numerical simulation, and non-spherical particles modeled as oblate spheroids are tracked as Lagrangian point-particles. The distribution, translation, rotation and orientation statistics of non-spherical particles have been explored in upward flow with gravity opposing, downward flow with aiding gravity, and channel flow in the absence of gravity. Parallel studies on spheres and fibers with different gravity directions in wall turbulence have been conducted by Marchioli et al. (2007) and Challabotla et al. (2016a, b), respectively. The results show that the upward flow configuration leads to a more uniform distribution of the flattest spheroids with modest inertia, and strong inertia reduces the impact of gravity and shape on the particle concentration. Though the gravity significantly influences the streamwise and wall-normal slip velocities of spheroids with the increasing inertia, the particle shape has little effect on the translational motion of disk-like particles, except for the mean wall-normal velocities. The velocity fluctuations of disk-like particles can mainly be ascribed to the inertia, and gravity as well as the particle shape only have a marginal effect. Moreover, the presence of gravity has a negligible influence on the rotation and orientation of disk-like particles, in spite of the fact that the spheroid shape has a remarkable influence in the near-wall regions. The common feature of near-wall disks and fibers is that both tend to align their long axis in the mean-shear plane. However, the long axis of a prolate spheroid is the symmetry axis, while the long axis of an oblate spheroid is perpendicalar to the symmetry axis. On the other hand, in the near-wall region, high-Stokes-number disks have a mean rotation

that is almost equal to the mean fluid rotation, and low-Stokes-number disks have a smaller rotation rate that decreases with larger asphericity. Additionally, the preferential alignment of oblate spheroids in the channel center is orthogonal to the fluid vorticity, which is opposite to that in the near-wall region.

The tendency of inertial particles to move towards regions of lower turbulence intensity made the gravity responsible for distinct distributions of particles. It is suggested that disk-like particles are more likely to locate at higher-speed fluid regions in the upward flow, and this tendency weakens with the large inertia and varies with the shape of spheroids. In addition, the Lagrangian statistics is suggested to explain the preferential alignment of spheroids in wall turbulence, as the symmetry axis of oblate spheroids is always observed to orient in the direction of Lagrangian compression. The actual gravity configuration in a turbulent channel, i.e. whether the flow is upward or downward, plays an important role in the transportation and separation of particles, as well as the optimization of industrial processes, and deserves further investigations.

Acknowledgements

References

Akhlaq, M., Sheltami, T.R., Mouftah, H.T., 2012. A review of techniques and technologies for sand and dust storm detection. Rev. Environ. Sci. Biotechnol. 11, 305-322.

Andersson, H.I., Soldati, A., 2013. Anisotropic particles in turbulence: status and outlook. Acta Mech. 224, 2219-2223.

Arcen, B., Taniere, A., Oesterle, B., 2006. On the influence of near-wall forces in particle-laden channel flows. Int. J. Multiph. Flow 32, 1326-1339.

Balachandar, S., 2009. A scaling analysis for point-particle approaches to turbulent multiphase flows. Int. J. Multiph. Flow 35, 801-810.

Balachandar, S., Eaton, J.K., 2010. Turbulent dispersed multiphase flow. Annu. Rev. Fluid Mech. 42, 111-133.

Brenner, H., 1964. The Stokes resistance of an arbitrary particle .4. Arbitrary fields of flow. Chem. Eng. Sci. 19, 703-727.

Byron, M., Einarsson, J., Gustavsson, K., Voth, G., Mehlig, B., Variano, E., 2015. Shape-dependence of particle rotation in isotropic turbulence. Phys. Fluids 27, 035101.

Challabotla, N.R., Nilsen, C., Andersson, H.I., 2015a. On rotational dynamics of inertial disks in creeping shear flow. Phys. Lett. A 379, 157-162.

Challabotla, N.R., Zhao, L., Andersson, H.I., 2015b. Shape effects on dynamics of inertia-free

spheroids in wall turbulence. Phys. Fluids 27, 061703.

Challabotla, N.R., Zhao, L., Andersson, H.I., 2015c. Orientation and rotation of inertial disk particles in wall turbulence. J. Fluid Mech. 766, R2.

Challabotla, N.R., Zhao, L., Andersson, H.I., 2016a. Gravity effects on fiber dynamics in wall turbulence. Flow Turbul. Combust. 97, 1095-1110.

Challabotla, N.R., Zhao, L., Andersson, H.I., 2016b. On fiber behavior in turbulent vertical channel flow. Chem. Eng. Sci. 153, 75-86.

Chen, J.C., Jin, G.D., Zhang, J., 2016. Large eddy simulation of orientation and rotation of ellipsoidal particles in isotropic turbulent flows. J. Turbul. 17, 308-326.

Eaton, J.K., 2009. Two-way coupled turbulence simulations of gas-particle flows using point-particle tracking. Int J Multiphase Flow 35, 792-800.

Gallily, I., Cohen, A.-H., 1979. On the orderly nature of the motion of nonspherical aerosol particles. II. Inertial collision between a spherical large droplet and an axially symmetrical elongated particle. J. Colloid Interface Sci. 68, 338-356.

Gillissen, J.J.J., Boersma, B.J., Mortensen, P.H., Andersson, H.I., 2007. On the performance of the moment approximation for the numerical computation of fiber stress in turbulent channel flow. Phys. Fluids 19, 035102.

Guasto, J.S., Rusconi, R., Stocker, R., 2012. Fluid mechanics of planktonic microorganisms. Annu. Rev. Fluid Mech. 44, 373-400.

Gustavsson, K., Einarsson, J., Mehlig, B., 2014. Tumbling of small axisymmetric particles in random and turbulent flows. Phys. Rev. Lett. 112, 014501.

Haller, G., 2015. Lagrangian coherent structures. Annu. Rev. Fluid Mech. 47, 137-162.

Han, C., 2012. Multiphase flow in polymer processing. Elsevier.

Harper, E.Y., Chang, I.D., 1968. Maximum dissipation resulting from lift in a slow viscous shear flow. J. Fluid Mech. 33, 209-225.

Jeffery, G.B., 1922. The motion of ellipsoidal particles immersed in a viscous fluid. Proc. R. Soc. Lond. Ser. A 102, 161-179.

Kleinstreuer, C., Feng, Y., 2013. Computational analysis of non-spherical particle transport and deposition in shear flow with application to lung aerosol dynamics—A review. J. Biomech. Eng. 135, 021008.

Kuerten, J.G.M., 2016. Point-particle DNS and LES of particle-laden turbulent flow - a state-of-the-art review. Flow Turbul. Combust. 97, 689-713.

Levin, E.J.T., McMeeking, G.R., DeMott, P.J., McCluskey, C.S., Carrico, C.M., Nakao, S., Jayarathne, T., Stone, E.A., Stockwell, C.E., Yokelson, R.J., Kreidenweis, S.M., 2016. Ice-nucleating particle emissions from biomass combustion and the potential importance of soot aerosol. J. Geophys. Res. 121, 5888-5903.

Li, Y., McLaughlin, J.B., Kontomaris, K., Portela, L., 2001. Numerical simulation of particle-

laden turbulent channel flow. Phys. Fluids 13, 2957-2967.

Loranger, E., Canonne, M., Daneault, C., Chabot, B., 2009. Effect of fibres on fluidized bed expansion parameters. Chem. Eng. J. 152, 530-536.

Lundell, F., Soderberg, L.D., Alfredsson, P.H., 2011. Fluid mechanics of papermaking. Annu. Rev. Fluid Mech. 43, 195-217.

Ma, L., Jones, J.M., Pourkashanian, M., Williams, A., 2007. Modelling the combustion of pulverized biomass in an industrial combustion test furnace. Fuel 86, 1959-1965.

Marchioli, C., Soldati, A., 2002. Mechanisms for particle transfer and segregation in a turbulent boundary layer. J. Fluid Mech. 468, 283-315.

Marchioli, C., Picciotto, M., Soldati, A., 2007. Influence of gravity and lift on particle velocity statistics and transfer rates in turbulent vertical channel flow. Int. J. Multiph. Flow 33, 227-251.

Marchioli, C., Soldati, A., Kuerten, J.G.M., Arcen, B., Taniere, A., Goldensoph, G., Squires, K.D., Cargnelutti, M.F., Portela, L.M., 2008. Statistics of particle dispersion in direct numerical simulations of wall-bounded turbulence: Results of an international collaborative benchmark test. Int. J. Multiph. Flow 34, 879-893.

Marchioli, C., Fantoni, M., Soldati, A., 2010. Orientation, distribution, and deposition of elongated, inertial fibers in turbulent channel flow. Phys. Fluids 22, 033301.

Marchioli, C., Soldati, A., 2013. Rotation statistics of fibers in wall shear turbulence. Acta Mech. 224, 2311-2329.

Marchioli, C., Zhao, L., Andersson, H.I., 2016. On the relative rotational motion between rigid fibers and fluid in turbulent channel flow. Phys. Fluids 28, 013301.

Marcus, G.G., Parsa, S., Kramel, S., Ni, R., Voth, G.A., 2014. Measurements of the solid-body rotation of anisotropic particles in 3D turbulence. New J. Phys. 16, 102001.

Mortensen, P.H., Andersson, H.I., Gillissen, J.J.J., Boersma, B.J., 2007. Particle spin in a turbulent shear flow. Phys. Fluids 19, 078109.

Mortensen, P.H., Andersson, H.I., Gillissen, J.J.J., Boersma, B.J., 2008a. On the orientation of ellipsoidal particles in a turbulent shear flow. Int. J. Multiph. Flow 34, 678-683.

Mortensen, P.H., Andersson, H.I., Gillissen, J.J.J., Boersma, B.J., 2008b. Dynamics of prolate ellipsoidal particles in a turbulent channel flow. Phys. Fluids 20, 093302.

Ni, R., Ouellette, N.T., Voth, G.A., 2014. Alignment of vorticity and rods with Lagrangian fluid stretching in turbulence. J. Fluid Mech. 743, 1-12.

Nilsen, C., Andersson, H.I., Zhao, L.H., 2013. A Voronoi analysis of preferential concentration in a vertical channel flow. Phys. Fluids 25, 115108.

Njobuenwu, D.O., Fairweather, M., 2013. Inertial particle behaviour in turbulent fluid flow. Proceedings of the 23rd European Symposium on Computer Aided Process Engineering – ESCAPE 23. Lappeenranta, Finland.

Njobuenwu, D.O., Fairweather, M., 2016. Simulation of inertial fibre orientation in turbulent flow. Phys. Fluids 28, 063307.

Pumir, A., Wilkinson, M., 2011. Orientation statistics of small particles in turbulence. New J. Phys. 13, 1-18.

Shapiro, M., Goldenberg, M., 1993. Deposition of glass-fiber particles from turbulent air-flow in a pipe. J. Aerosol Sci. 24, 65-87.

Siewert, C., Kunnen, R.P.J., Meinke, M., Schroder, W., 2014. Orientation statistics and settling velocity of ellipsoids in decaying turbulence. Atmos. Res. 142, 45-56.

Soldati, A., Marchioli, C., 2009. Physics and modelling of turbulent particle deposition and entrainment: Review of a systematic study. Int. J. Multiph. Flow 35, 827-839.

Tominaga, Y., Stathopoulos, T., 2013. CFD simulation of near-field pollutant dispersion in the urban environment: A review of current modeling techniques. Atmos. Environ. 79, 716-730.

Uijttewaal, W.S.J., Oliemans, R.V.A., 1996. Particle dispersion and deposition in direct numerical and large eddy simulations of vertical pipe flows. Phys. Fluids 8, 2590-2604.

Voth, G.A., 2015. Disks aligned in a turbulent channel. J. Fluid Mech. 772, 1-4.

Voth, G.A., Soldati, A., 2017. Anisotropic particles in turbulence. Annu. Rev. Fluid Mech. 49, 249–276.

Zhang, H., Ahmadi, G., Fan, F.G., McLaughlin, J.B., 2001. Ellipsoidal particles transport and deposition in turbulent channel flows. Int. J. Multiph. Flow 27, 971-1009.

Zhao, F., van Wachem, B.G.M., 2013. Direct numerical simulation of ellipsoidal particles in turbulent channel flow. Acta Mech. 224, 2331-2358.

Zhao, F., George, W.K., van Wachem, B.G.M., 2015. Four-way coupled simulations of small particles in turbulent channel flow: The effects of particle shape and Stokes number. Phys. Fluids 27, 083301.

Zhao, L., Marchioli, C., Andersson, H.I., 2012. Stokes number effects on particle slip velocity in wall-bounded turbulence and implications for dispersion models. Phys. Fluids 24, 021705.

Zhao, L., Andersson, H.I., Gillissen, J.J.J., 2013a. Interphasial energy transfer and particle dissipation in particle-laden wall turbulence. J. Fluid Mech. 715, 32-59.

Zhao, L., Andersson, H.I., Gillissen, J.J.J., 2013b. On inertial effects of long fibers in wall turbulence: fiber orientation and fiber stresses. Acta Mech. 224, 2375-2384.

Zhao, L., Marchioli, C., Andersson, H.I., 2014. Slip velocity of rigid fibers in turbulent channel flow. Phys. Fluids 26, 063302.

Zhao, L., Challabotla, N.R., Andersson, H.I., Variano, E.A., 2015. Rotation of nonspherical particles in turbulent channel flow. Phys. Rev. Lett. 115, 244501.

Zhao, L., Andersson, H.I., 2016. Why spheroids orient preferentially in near-wall turbulence. J. Fluid Mech. 807, 221-234.